*

Simultaneous removal of soot and NO_x over Ruthenium-based catalysts

Roberto Matarrese[1], Eleonora Aneggi[2], Lidia Castoldi[1*], Jordi Llorca[3],

Alessandro Trovarelli[2], Luca Lietti[1]

[1]*Politecnico di Milano, Dipartimento di Energia, via La Masa 34,*

20156 Milano, Italy

[2]*Università di Udine, Dipartimento di Chimica, Fisica e Ambiente, via Cotonificio 108,*

33100 Udine, Italy

[3]*Institut de Tècniques Energètiques and Centre for Research in Nanoengineering, Universitat*

Politècnica de Catalunya, 08028 Barcelona, Spain

*to whom correspondence should be addressed.

Tel. +39 02 2399 3255

Fax. +39 02 2399 8566

e-mail: lidia.castoldi@polimi.it

Abstract

Ruthenium-based materials are investigated for the simultaneous removal of soot and NO_x and their behaviour is compared with that of model Pt-Ba/Al_2O_3 and Pt-K/Al_2O_3 catalysts.

The materials, 1%wt Ru – 10%wt AM/MO (AM= Ba or K; MO = $Ce_{0.8}Zr_{0.2}O_2$, ZrO_2, Al_2O_3), have been prepared by incipient wetness impregnation and characterized by BET, XRD, HRTEM and TPR experiments. The catalytic activity for diesel soot combustion is studied under loose contact conditions by means of TPO (Temperature Programmed Oxidation) while the reactivity in the NO_x removal is investigated by Isothermal Concentration Step Change experiments.

All the ruthenium-based formulations are active in the combustion of diesel soot, particularly potassium-doped materials that show low onset temperatures, near 230 °C. The catalytic activity in the simultaneous removal of soot and NO_x shows that Ru-based catalysts are very efficient in the oxidation of soot also under isothermal conditions and that their NO_x removal capacity (i.e. storage capacity) is almost comparable to that of traditional Pt-based LNT systems. However, the NO_x reduction efficiency of the Ru-containing catalysts is lower than that of traditional LNT Pt-based catalysts.

Keywords: LNT, DPNR, ruthenium, potassium, soot oxidation, NO_x removal.

1. INTRODUCTION

The environmental problems associated with the use of diesel engines, and the strengthening of the regulations concerning pollutant emissions in the transport field, have recently led to focus the attention on new technologies able to reduce the emissions of NO_x and particulate matter (PM or soot) [1-4].

To date, the most effective and widely applied post-treatment technology for particulate matter is the diesel particulate filter (DPF) [2, 3, 5], able to remove more than 90% [4]. In order to avoid pressure drop increase, filters need to be periodically regenerated and one of the most favored solutions is the catalytic oxidation of particulate matter.

The efficiency in the reduction of nanoparticles and the low temperature regeneration still represent big challenges in the soot oxidation process. The research is focused on the design and the achievement of active catalysts, deposited on the filter media, allowing the passive regeneration to occur in a continuous or periodic manner during the regular operation of the engine typically in the 300-400°C temperature range [4]. In the last decade, several formulations were proposed as soot oxidation catalyst [6] and the most promising are based on ceria-doped materials [7-15], transition metals (such as Ag, Cu, V, Mo, Co, Mn or Fe) [16-21], systems containing a combination of transition and alkaline or alkaline earth metals [16, 22] or perovskites [23, 24].

The combined reduction of NO_x and soot is also a key issue. Over the years, many technologies have been developed for reducing nitrogen oxides and to remove simultaneously NO_x and particulate matter. The combined removal of NO_x and soot dictates the use of a combination of selective catalytic reduction or lean NO_x adsorbers with catalytic filter traps. Example is the BlueTEC® system [25] which includes a DOC (to oxidize HC and CO) followed by a non

catalytic DPF (for the PM removal), a LNT system (Lean NO_x Trap, for the storage/reduction of the NO_x by alternating lean-rich phase), and finally a SCR unit to adsorb NH_3 produced by the LNT unit and then reduce the residual NO_x during the lean phase. The use of integrated DOC-DPF-LNT-SCR systems has been proposed in different configurations in order to exploit potential synergisms among the various devices.

An innovative solution has been developed by the Toyota group [26, 27], consisting of a DPF/LNT integrated after-treatment solution, known as DPNR (Diesel Particulate NO_x Reduction). This system consists of a new catalytic filter and a new diesel combustion technology, reducing both particulate and NO_x emissions. The catalytic converter for DPNR is a porous ceramic filter coated with a catalytic layer constituted by a high surface area support (e.g. -alumina), a noble metal (Pt), and an alkaline or earth-alkaline metal oxide, with a high NO_x-storage capacity. These catalytic systems work under cyclic conditions, alternating long lean phases with short regeneration phases in rich condition: during lean phase the NO_x produced by the engine are adsorbed on the alkaline or earth-alkaline metal oxide component (with nitrite-nitrate species formation), while during rich phase the nitrate-nitrite species are reduced to molecular nitrogen by CO, H_2 and unburnt HC. The particulate matter removal occurs mainly under lean conditions by oxygen and NO_2 formed upon NO oxidation over the noble metals. Pt-Ba/Al_2O_3 and Pt-K/Al_2O_3 have been used in this application, and several studies have been devoted to the understanding of catalytic activity, reaction mechanisms and interactions between the De-soot and De-NO_x functions [28-31]. In particular, Pt-Ba/Al_2O_3 and Pt-K/Al_2O_3 catalysts exhibit similar De-NOx activity although the K-containing system showed significantly higher activity for soot combustion [32-35].

More recently the development of noble metal-free formulations have been attempted and promising results were found for Ag-based materials [36]. These formulations decrease the soot oxidation temperature in presence of NO/O_2 with an onset temperature near 250°C [18, 36]. Moreover, the silver-containing catalysts are active in the simultaneous removal of soot and NO_x, when alternating lean-rich phases according to the typical DPNR strategy. These catalysts have shown a remarkable storage capacity, comparable to that of the traditional $Pt\text{-}Ba/Al_2O_3$ LNT catalyst, but a limited selectivity to N_2 during the rich phase (i.e. during the reduction of the stored NO_x).

In the present study we have investigated a different class of Pt-free catalysts based on ruthenium. Ruthenium-based materials have been widely studied as redox catalyst for several reactions such as partial oxidation of methane [37, 38], catalytic wet air oxidation [39, 40], oxidation of organic compound [41-44], carbon monoxide oxidation [45, 46] and, more recently, for soot oxidation as well [45, 47-52]. This prompted us to investigate for the first time the behavior of ruthenium-containing formulations according to the DPNR concept, and to compare their activity with that of $Pt\text{-}Ba/Al_2O_3$ and $Pt\text{-}K/Al_2O_3$ catalysts. Accordingly, we have developed two series of materials (i.e. Ru–Ba/MO and Ru–K/MO - MO = $Ce_{0.8}Zr_{0.2}O_2$, ZrO_2, Al_2O_3) and we have investigated their catalytic activity in soot combustion (under loose contact conditions) by means of TPO, NO_x removal and combined NO_x and soot abatement by lean/rich cycles.

2. EXPERIMENTAL

2.1 Catalysts preparation and characterization

Ceria–zirconia solid solution was prepared by coprecipitation at pH 9.5 starting from nitrates (Treibacher Industrie AG) in the presence of H_2O_2 (Sigma Aldrich) and using ammonia (Sigma

Aldrich) as precipitating agent [53]. The filter cake was then washed with distilled water, followed by drying and calcination at 773 K. Zirconium oxide was obtained from $Zr(OH)_4$ (MEL Chemicals) by calcination at 500 °C for 3 h. The materials were prepared by incipient wetness impregnation of ceria-zirconia solid solution, zirconia and alumina (Sasol Germany GmbH) with aqueous solutions of ruthenium nitrosyl nitrate, barium acetate and potassium nitrate (purchased by Sigma Aldrich) in order to obtain the following two series of materials: Ru(1% w/w)-Ba(10% w/w)/MO and Ru(1% w/w)-K(10% w/w)/MO (MO = $Ce_{0.8}Zr_{0.2}O_2$, ZrO_2, Al_2O_3). After impregnation, the samples were dried at 100 °C overnight and calcined under air at 500 °C for 3h.

Textural characteristics were measured according to the B.E.T. method by N_2 adsorption - desorption at -196°C, using a Tristar 3000 gas adsorption analyzer (Micromeritics). Structural features of the catalysts were investigated by powder X-ray diffraction analysis (XRD). Diffractograms were recorded on a Philips X'Pert diffractometer (equipped with a real time multiple strip detector) operated at 40kV and 40mA with Ni-filtered Cu-Kα radiation using a step size of 0.02° and a counting time of 40 s per angular abscissa in the range 20°-80°. The Philips X'Pert HighScore software was used for phase identification.

For high-resolution transmission electron microscopy studies (HRTEM), a JEOL JEM 2010F electron microscope equipped with a field emission gun was used working at an accelerating voltage of 200 kV. Samples were dispersed in ethanol in an ultrasonic bath and a drop of supernatant suspension was poured onto a holey carbon coated grid and dried completely before measurements.

Temperature programmed reduction (TPR) experiments with a AutoChem II 2920 instrument (Micromeritics) have been used to measure the redox behavior of the catalytic materials.

Samples (50-60 mg) were heated from room temperature to 800°C at a constant rate (10°C/min) in a U-shaped quartz reactor, under a flowing hydrogen/nitrogen mixture (35 ml/min, 4.5% H_2 in N_2) while monitoring the hydrogen consumption with a TCD detector. The outlet gas composition was also followed by an on line quadrupole mass-spectrometer (Omnistar, Balzers Instruments).

2.2 Catalytic tests and methods

The activity in the soot combustion, NO_x removal and the combined NO_x and soot abatement has been investigated.

The catalytic activity for the combustion of soot was determined from peak-top temperature (T_p) during temperature programmed oxidation (TPO) experiments of catalyst-soot mixtures. A weight soot/catalyst ratio of 1:20 was used; the mixture has been obtained by mixing each catalyst with soot (Printex-U, Degussa AG) with a spatula for 2 minutes realizing the so-called loose contact between catalyst and soot. In the TPO measurements, 20 mg of the above mixture were heated at a constant rate (10°C/min) in a quartz reactor under O_2/N_2 (10% O_2 v/v, balance N_2; total flow 0.5 l/min) or $O_2/NO/N_2$ gas flow (10% O_2 v/v + 500 ppm NO, balance N_2; total flow 0.5 l/min). The catalyst temperature was measured by a chromel-alumel thermocouple, located on the catalyst bed. The outlet gas composition (i.e. CO, CO_2, NO and NO_2) was measured by FT-IR gas analyzers (MultiGas 2030, MKS). Reproducibility of results was verified by running several TPO experiments on similar samples and the results in terms of T_p were always within ± 3°C.

The reactivity tests for the removal of NO_x and then for the simultaneous removal of NO_x and soot were performed in a micro flow-reactor apparatus consisting of a quartz tube reactor (7 mm

i.d.) connected to a mass spectrometer (QMS 200, Pfeiffer Vacuum), a micro-GC (R3000, SRA) and an FT-IR analyzer (MultiGas 2030, MKS) for the on-line analysis of the outlet gases (NO, NO_2, N_2, H_2, O_2, CO, CO_2, N_2O and NH_3). 60 mg of catalyst was used in each run. The catalyst (without soot) has been conditioned by performing a temperature programmed desorption (TPD) experiment followed by some storage/regeneration cycles, until a reproducible behavior was obtained, according to the ICSC procedure described below. This typically required 3-4 adsorption/reduction cycles. TPD has been carried out from room temperature up to 500°C (10°C/min) in He and holding at this temperature 20 min. Then the temperature has been decreased to 350°C and lean/rich cycles have been performed by alternating rectangular step feeds of NO (1000 ppm) + 3% v/v O_2 in flowing He (lean phase) with steps of H_2 (4000 ppm) in He, with an He purge in between (Isothermal Concentration Step Change experiments, ICSC). TPD have been performed after a sequence of lean/rich cycles in order to complete catalysts regeneration (i.e to remove any residual NO_x stored species).

The $DeNO_x$ – DeSoot activity has been tested for the same catalysts with similar ICSC experiments using 66 mg of soot-catalyst loose mixture (composed by 59.4 mg of the bare catalyst and 6.6 mg of soot) and performing 7 storage – reduction cycles and subsequently oxidizing the residual soot by Temperature Programmed Oxidation (TPO) in 3% v/v O_2 in He from 350°C up to 750°C (10°C/min).

3. RESULTS AND DISCUSSION

3.1. Structural and morphological characterization of materials

Composition and BET surface area of the ruthenium-based catalysts and the supports are reported in Table 1. Surface area values indicate that deposition of ruthenium and alkaline or

alkaline-earth metals reduces available surface compared to bare supports with a larger effect for potassium containing materials. In fact, the addition of metal oxides with high specific weight and low porosity over high-surface area supports typically results in a significant decrease of the surface area [54, 55].

The structural and morphological characteristics of the catalysts were studied by XRD, HRTEM, TG and TPR measurements. X-ray diffraction profiles are shown in Figure 1. For all the materials, peaks belonging to the support are clearly observed. The fluorite phase was detected for ceria-zirconia solid solution, as expected for this Ce/Zr ratio [9]; zirconia samples crystallize in a mixture of monoclinic and tetragonal phase (around 95% and 5%, respectively) while for alumina XRD reveals the presence of γ-Al_2O_3 phase. In addition, orthorhombic whiterite ($BaCO_3$) and potassium nitrate (KNO_3) phases were detected, respectively for barium and potassium doped samples, in agreement with several studies [56-59]. No evidence of the presence or ruthenium crystallites (metallic or oxide) was obtained. This could be due either to the low amount of Ru and to the high dispersion of the ruthenium phase over the supports. An excellent dispersion of Ru nanoparticles was confirmed by HRTEM measurements (Figure 2) performed on the as prepared catalysts to better elucidate the morphology and distribution of the species occurring in the materials.

Figure 2A shows a representative image of Ru-Ba/CZ. The sample contains $Ce_{0.8}Zr_{0.2}O_2$ crystallites of about 5-10 nm in size and a good dispersion of metallic Ru nanoparticles, the largest ones measuring about 3-5 nm. It is possible to recognize that there is a good contact between the $Ce_{0.8}Zr_{0.2}O_2$ support and the Ru nanoparticles. Areas marked “a” and “b” correspond to a $Ce_{0.8}Zr_{0.2}O_2$ crystallite (the spot at 3.0 Å corresponds to the (111) planes) and a Ru nanoparticle (the spot at 2.1 Å is ascribed to the (002) planes of metallic Ru). In Figure 2B,

image of Ru-Ba/Zr sample is reported, where several Ru clusters are marked by arrows. The sample is constituted by ZrO_2 particles with a round-shape morphology, measuring about 15-20 nm in size. The support particles are completely crystalline. The Ru clusters are very well dispersed over the support and measure less than 0.5 nm. Lattice fringes at 2.84 Å correspond to the (111) crystallographic plane of monoclinic ZrO_2.

Also in the case Ru-Ba/Al, the sample contains small particles of support of about 5-10 nm in size and Ru metal nanoparticles measuring up to 3-4 nm. Figure 2C reports a general view as well as an enlargement to show a Ru nanoparticle; lattice fringes at 2.33 Å correspond to the (100) planes of metallic Ru.

The Ru-K/CZ sample is comprised by support crystallites with abundant voids, as it can be seen in the general images depicted in Figure 2D. The support particles range mostly from 10 to 50 nm. At high magnification the Ru nanoparticles can be seen (some of them are marked by arrows). It is worth to note that the dispersion of Ru is excellent and the Ru nanoparticles are very homogeneous in size, measuring about 0.5 nm. This value is at the limit of the microscope capability and the existence of smaller Ru clusters cannot be ruled out. Given the small size of the Ru nanoparticles it is not possible to obtain lattice fringe images which would demonstrate unambiguously that the dark spots correspond really to the Ru nanoparticles, but the existence of such dark spots cannot be due to the CZ support and cannot be ascribed to the presence of potassium. Figure 2E shows Ru-K/Zr material, that closely resemble Ru-Ba/Zr catalyst, for the morphology and size of the support particles as well as the size of Ru clusters (marked by arrows in the high magnification inset). Again, they are very well dispersed over the support and measure less than 0.5 nm. In Figure 2E lattice fringes at 3.64 Å correspond to the (110) crystallographic planes of monoclinic ZrO_2. Ru-K/Al sample is constituted by alumina support

particles of about 10-20 nm in size. In the same image (Figure 2F) several Ru nanoparticles are marked by arrows as well. In this sample the distribution of Ru particle size ranges from about 0.5 nm to 1.5 nm. In the high magnification inset, two different images recorded under different focus conditions corresponding to the same area show the presence of Ru clusters (inside the dashed circles).

HRTEM analysis focused the presence, for all the catalysts, of metallic ruthenium nanoparticles (from 0.5 to 5 nm in size, depending on the samples) and an excellent dispersion of Ru over the supports.

Reducibility of materials has also been investigated by H_2-temperature programmed reduction (Figure 3). For all the catalysts it is possible to recognize a major broad region of hydrogen consumption at low temperatures (at 150 °C for Ba-based samples and around 300-350 °C for K-containing materials) and a small H_2 consumption peak at higher temperature (600-750 °C). The first reduction peak is associated to the formation of methane due to the reduction of carbonate (as shown in the inset of Figure 3 for the Ru-K/CZ catalyst as a representative example). Higher amount of carbonate species are found in K-based samples, likely due to the formation of carbon-oxygen complexes (C-O-K) over K-doped materials [60-62]. In the case of ceria-based materials, i.e. Ru-Ba/CZ and Ru-K/CZ, the consumption of hydrogen at low temperature is higher if compared to the ZrO_2 and Al_2O_3 supported materials, and might be associated to the partial reduction of surface cerium species. On the other hand, peaks at higher temperature (600-750°C) are correlated with the decomposition of nitrates/nitrites. Hence H_2 consumption due to reduction of ruthenium species is not clearly distinguished in the TPR profile, in agreement with HRTEM measurements that evidenced the presence of very well dispersed metallic ruthenium nanoparticles.

Release of CO_2 and NO_x from carbonate/nitrate decomposition has also been confirmed by TGA experiments, which show weight loss in the region around 150 and 600 °C corresponding to desorption of CO_2 and NO_x respectively. The release of CO_2 at low temperature (150-200 °C) could be due to the decomposition of surface carbonate species on alkaline and alkaline-earth metals [62].

3.2. Soot oxidation activity

Figure 4A and 4B summarize the results for TPO experiments carried out in O_2/N_2 and in $NO/O_2/N_2$ atmosphere.

Ba-doped samples are moderately active in O_2 atmosphere, while the presence of NO significantly affects their catalytic activity; this is true especially for Ru-Ba/CZ catalyst where a decrease of almost 90 °C is observed, suggesting a specific role of the support in the soot oxidation.

On the other hand, the activity of K-based materials is not influenced by the presence of NO in the reaction atmosphere. Moreover, the activity is not correlated with the nature of the supports and all the K-containing catalysts exhibit a peak temperature at around 390 °C.

A comparison with the traditional Pt-based LNT materials (Figure 4B) shows that the addition of Ru is particularly beneficial in NO-assisted soot oxidation with a decrease of combustion temperature of around 40 °C and 65 °C, respectively for Ba and K-doped formulations. Beside the oxidation temperature, another important parameter to evaluate is the onset temperature that is obtained in correspondence of 20 ppm of CO_2 produced by the oxidation process. In all investigated samples a remarkable decrease of the onset temperature is achieved by adding ruthenium: comparing Ba-Al-doped materials, Ru catalyst exhibits an onset temperature of 320

°C vs 425 °C for Pt catalyst, while the substitution of Ba with K induces a further decrease of T_{onset} down to 235 °C confirming the excellent soot oxidation properties of these formulations.

Several studies pointed out the interesting activity of ruthenium over different supports in carbon combustion and in the oxidation of methanol and organic compounds. In some cases, the mechanism of reaction is based on the presence of RuO_2 species [48, 51], while in others the presence of metallic ruthenium seems to enhance the activity, possibly due to the formation of active oxygen species [44, 63, 64]. In our case, HRTEM measurements (Figure 2) detected metallic ruthenium nanoparticles very well dispersed over the support for all the materials. Over these nanoparticles a dissociative adsorption of oxygen could take place generating active oxygen [41] and promoting soot oxidation activity. Catalytic activity tests highlighted a remarkable decrease of the onset (T_{onset} in the range 220-235 °C) and peak oxidation temperature ($T_p \approx$ 380-397 °C) for all K-based materials compared to traditional formulations, and this suggests a synergic effect of K and Ru that boosts the combustion of carbon particles at lower temperature.

3.3. NO_x storage–reduction activity in the absence of soot

The results obtained in the ICSC experiments carried out over fully conditioned Ru-Ba- and Ru-K-based catalysts are shown in Figure 5 and 6, respectively. The figures show the NO,NO_2, NO_x (i.e. NO + NO_2) concentration profiles during the lean phase, and the H_2, N_2 NO, NH_3, N_2O concentration profiles measured during the rich phase. The TPD run carried out at the end of the sequence is also reported for the Ru-Ba-based catalysts (Figure 5).

In the case of Ru–Ba/Al catalyst (Figure 5A), upon the NO step addition (at t = 0 s) a delay near 120 s is observed in the NO outlet concentration, which indicates an initial complete NO_x uptake.

The parallel evolution of NO_2 is observed, which is related to the oxidation of NO by O_2 at Ru sites [65 and refs herein reported]. After breakthrough, the concentrations of both NO and NO_2 increase with time and eventually reach a steady state level. Of note, the NO_2 concentration measured at steady state is near the chemical equilibrium indicating the high NO oxidation capacity of the catalyst (i.e. higher than that of typical Pt-Ba/Al_2O_3 and Pt-K/Al_2O_3 LNT catalytic systems [66, 67]).

Adsorbed amounts of NO_x near 0.37 mmol/g_{cat} have been estimated at the end of the NO dose, values which are only slightly lower than those reported in literature for typical LNT catalytic systems [67, 68]. When the NO and O_2 inlet concentrations are switched off (t = 1770 s and 2400 s, respectively) a tail (and a puff in correspondence of O_2 closure) is observed in the NO concentration profile, due to the desorption of weakly adsorbed NO_x species [69 and refs herein reported] causing a decrement of roughly 53% in the amount of stored NO_x.

After NO and oxygen shutoff, hydrogen is admitted to the reactor (t = 3210 s) in order to regenerate the catalyst surface. As opposed to typical LNT catalytic systems [69-71] the regeneration of the catalysts is very slow and not so efficient. As a matter of fact, H_2 consumption is not complete and its concentration immediately increases with time until the inlet value of 4000 ppm. N_2 evolution is observed upon H_2 admission showing a peak and then slowly decreasing with time. Small amounts of ammonia are also observed leading to nitrogen selectivity near 96%. The catalyst is not fully regenerated at the end of the reduction phase (t = 5100 s), as indicated by the subsequent TPD during which desorption of NO is detected.

In Figure 5B the storage/reduction phases of the fully conditioned Ru–Ba/Zr catalyst are reported. Upon the NO step addition, NO is immediately observed at the reactor outlet along with minor amounts of NO_2. Then the NO_x concentration immediately reaches the inlet value

indicating that this catalyst is not able to accomplish any significant NO_x uptake. Accordingly, the amounts of stored NO_x are very low, near 0.05 mmol/g_{cat}. During the subsequent regeneration step with H_2 the reduction of stored NO_x is mostly negligible, as indicated by the very low amounts of nitrogen and ammonia detected at the reactor outlet. Most of the stored NO_x species are decomposed to NO during the subsequent TPD.

Finally, in the case of the Ru–Ba/CZ catalyst (Figure 5C), upon NO admission to the reactor (t = 0 s), NO is immediately observed at the reactor outlet. NO_2 formation due to the oxidation of NO in the presence of oxygen and catalyzed by Ru also takes place. However, the NO_2 concentration measured at steady state is lower than that measured over Ru–Ba/Al pointing out the minor NO oxidation capacity of Ru–Ba/CZ catalyst. Of note, after breakthrough, the NO_x concentration increases very slowly with time indicating the high storage capacity of this system. The overall amount of NO_x stored onto the catalyst surface is near 0.41 mmol/g_{cat}, which is similar to that of the Ru–Ba/Al catalyst (i.e. 0.37 mmol/g_{cat}). Upon NO and O_2 shut off, the desorption of weakly adsorbed NO_x is occurring although less evident than the Ru-Ba/Al sample, being near 30% vs. 53% for Ru–Ba/Al.

After NO_x adsorption and helium purge, the reduction of the stored NO_x has been carried out also in this case. Upon H_2 addition (at t = 0s), an hydrogen spike is observed (1500 ppm) followed by an increase up to the inlet value. Nitrogen is formed along with minor amounts of NO and ammonia resulting in a N_2 selectivity near 83%. No desorption of N-containing species is observed during the subsequent TPD which indicates that all the stored NO_x species have been removed and that the catalytic surface is fully regenerated.

NO_x storage/reduction experiments were also performed in the case of Ru-K-based catalyst and the results are shown in Figure 6A, B and C for Ru-K/Al, Ru-K/Zr and Ru-K/CZ, respectively.

As apparent from Figure 6A the NO_x storage behavior of Ru-K/Al is qualitatively similar to that of Ru–Ba/Al (see Figure 5A), although a lower NO oxidation capility is observed. In fact, upon NO admission to the reactor (t = 0), both NO and NO_2 are seen at the reactor outlet with a delay of ca. 150 s. Their concentration then increase with time, approaching the asymptotic concentrations corresponding to the NO inlet concentration. The NO_x stored amounts up to saturation are close to 0.6 mmol/g_{cat}, i.e. higher than of Ru–Ba/Al (0.37 mmol/g_{cat}). The stored NO_x species are rather stable, as pointed out by the small tail that is observed at the NO shut off.

After adsorption, the stored NO_x have been reduced by feeding hydrogen (4000 ppm). As for Ru–Ba/Al, the H_2 consumption is not complete and its concentration immediately increases with time until the inlet value of 4000 ppm. Moreover, as opposite to what observed for Ru-Ba/Al where N_2 was the main reduction product, a huge amount of NO is observed in this case along with minor amounts of nitrogen and ammonia. Accordingly, the selectivity to N_2 is rather low, near 32% (vs. 96% for Ru–Ba/Al). Also in this case the catalyst is not fully regenerated during reduction, as indicated by the subsequent TPD (not shown in the figure) during which the desorption of NO is detected.

The NO_x storage behavior of both Ru-K/Zr and Ru-K/CZ (see Figure 6B and C) is similar to that observed for Ru-K/Al. In both samples a significant NO_x storage is observed, at variance with Ba-based catalysts. In particular the Zr-supported catalyst shows a high storage capacity close to 0.77 mmol/g_{cat} (vs. 0.6 mmol/g_{cat} and 0.26 mmol/g_{cat} for Ru-K/Al and Ru-K/CZ, respectively).

The reduction behavior of Ru-K/CZ (Figure 6C) is similar to that observed for Ru-K/Al: NO is the main reduction product leading to a low N_2 selectivity of ca. 41%. A slightly different picture is observed in the case of Ru-K/Zr (Figure 6B). Again the initial evolution of NO is observed but then, at higher reduction time also low amounts of N_2O and finally an high production of N_2 are

seen at the reactor outlet so that a nitrogen selectivity near 71% has been estimated in this case at the end of the reduction phase. Also for Ru-K/Zr and Ru-K/CZ the regeneration is not efficient, as pointed out by the subsequent TPD during which the desorption of NO has been detected.

The observed temporal evolution of the reduction products (i.e. nearly complete NO selectivity at the beginning of the rich phase and conversely high N_2 selectivity at the end) can be related to the different oxidation state of ruthenium during the regeneration process. It is likely that the initial presence of Ru-O sites, that are not efficiently reduced to metal Ru, may result in the formation of mainly NO among the reduction products. Besides, with the increasing exposure time under rich conditions O-adatoms can be scavenged from Ru (i.e. Ru is kept in an increasing reduced state) giving N_2O and finally N_2 instead of NO.

These results clearly show that the substitution of Ba with K not only affects the NO_x storage behavior of the investigated Ru-based catalysts but also their reduction activity.

3.4. Simultaneous removal of NO_x and soot

NO_x adsorption–reduction experiments have been carried out at 350°C also in the presence of soot in order to investigate the capability of both Ru-Ba/ and Ru-K/supported catalysts to accomplish the simultaneous removal of NO_x and soot. The experiments have been carried out only in the case of Ru–Ba/Al_2O_3 and Ru–Ba/CZ80, i.e. among the Ba-based catalysts the morphologies that have shown the best NO_x storage performances in the absence of soot, and the results are shown in Figure 7.

In the case of Ru–Ba/Al_2O_3/soot mixture (Figure 7A), the evolution of NO and NO_2 is qualitatively similar to those observed for the soot-free catalyst. Upon NO addition to the reactor (t = 0 s) the NO_x outlet concentration shows a dead time and then increases approaching the

asymptotic values corresponding to the NO inlet concentration. However, significant differences are apparent with respect to the soot-free catalyst. In the presence of soot the NO_x dead time is increased (from ca. 120 to ca. 200 s) and after breakthrough the NO_x concentration increases, but slowly if compared to the soot-free system. Moreover, a lower NO_2/NO ratio is observed at the end of the pulse, near catalyst saturation. The amounts of NO_x that have been stored onto the catalyst surface are 0.64 mmol/g_{cat} vs. 0.37 mmol/g_{cat} in the absence of soot which indicates an increased storage capacity of the catalyst in the presence of soot. This is rather surprising since in all the other investigated samples (e.g. the reference Pt-Ba/Al_2O_3 [72] and Pt-K/Al_2O_3 [32] LNT catalytic systems) a negative effect of soot on the NO_x storage activity has been found.

The storage of NO_x is accompanied by the evolution of CO_2 which is representative of the soot combustion activity having operated in a CO_2-free environment. The soot combustion activity of the Ru–Ba/Al is much higher than that of the reference Pt–Ba/Al_2O_3 LNT catalysts [34], pointing out the high activity of Ru. In particular, differently from Pt–Ba/Al_2O_3, the evolution of CO_2 is observed in presence of only oxygen, before the NO addition. Then, upon NO admission (t = 0s), the CO_2 concentration further increases showing a maximum of 900 ppm and then its concentration reaches a constant value of 750 ppm till the end of the NO dose.

In the presence of NO, soot oxidation can be ascribed to NO_2, formed upon NO oxidation over Ru sites, according to reaction (1):

$$2\ NO_2 + C \rightarrow 2\ NO + CO_2 \qquad (1)$$

Accordingly, the NO_2 concentration measured at steady state is lower in the presence of soot than over the soot-free catalyst, indicating the participation of NO_2 in the combustion of soot. However the observed CO_2 production is higher than that expected from the stoichiometry of reaction (1). As proposed for Pt-based catalysts [73] this could be explained with to the so-called

"NO recycle", i.e. to the oxidation of NO produced according to reaction (1) to NO_2, catalyzed by Ru. In addition, it is also well known that the presence of NO_2 enhances soot oxidation by oxygen [74, 75].

Moreover, the evolution of CO_2 in presence of only oxygen (i.e. before and after the NO dose) strongly suggests a direct role of the ruthenium in the oxidation of soot which is possibly superimposed to the soot combustion activity by NO_2. Finally, in line with previous works [72, 76], the possible participation of the stored NO_x in soot combustion via a direct surface reaction cannot be excluded.

Upon NO and oxygen shutoff at the end of the adsorption phase (Figure 7A), a release of NO_x takes place due to the desorption of the previously stored NO_x species. Both desorption contributions are very similar to those observed over the soot-free catalyst, indicating that soot doesn't significantly affect the stability of the NO_x species stored over Ru–Ba/Al, at variance with that observed over typical Pt-Ba/Al_2O_3 [72] and Pt-K/Al_2O_3 LNT catalysts.

The reduction of the NO_x adsorbed species in the presence of soot does not show significant differences with respect to the soot-free catalyst (compare Figures 7A and 5A). Upon hydrogen admission (t = 3030 s), the H_2 consumption is not complete and its concentration immediately increases with time until the inlet value of 4000 ppm. As for the soot-free case, N_2 is the main reduction production. However, in addition to the formation of ammonia, also the evolution of NO is observed resulting in a nitrogen selectivity near 68% (vs. 96% the soot-free catalyst).

The behavior of Ru–Ba/CZ catalyst in the presence of soot has also been tested and the results are reported in Figure 7B. Unlike Ru–Ba/Al, the NO_x storage capacity of the CZ-supported catalyst slightly decreases in the presence of soot. The NO_x breakthrough is still zero and then the NO_x concentration increases more rapidly than over the soot-free case so that the amount of

stored NO_x is lower (0.32 mmol/g_{cat} vs. 0.41 mmol/g_{cat}). Upon NO admission, production of CO_2 is detected at the reactor outlet although in lower amounts with respect to Ru-Ba/Al, indicating the lower soot combustion activity of this catalyst. In fact, during the lean phase, 9% of soot has been oxidized ,vs. 22% in the case of Ru-Ba/Al. As for the Al_2O_3-supported catalyst, the reduction of the stored NO_x (i.e. catalyst regeneration) is not significantly affected by the presence of soot, if one neglects a small decrease in the N_2 selectivity (from 83% in the absence of soot down to 74% in the presence of soot).

The $DeNO_x$-DeSoot activity has been studied also in the case of Ru-K-based catalyst mixed with soot and the results are shown in Figure 8A, B and C for Ru-K/Al, Ru-K/Zr and Ru-K/CZ, respectively.

The general features of the storage phase previously described in the absence of soot are confirmed, indicating that all the investigated Ru-K-based catalysts are able to store NO_x, even in the presence of soot. Notably, in all cases, the NO_x outlet concentration shows a dead time and then increases with time. Upon NO admission (t = 0 s) all the catalysts show a NO_x breakthrough higher than that observed over the corresponding soot-free systems. Moreover, after breakthrough, the NO_x concentration increases more slowly than in the absence of soot. The NO_x stored at the end of adsorption phase are close to 1.1 mmol/g_{cat}, 1.6 mmol/g_{cat} and 1.7 mmol/g_{cat} for Ru-K/Al, Ru-K/Zr and Ru-K/CZ, respectively, which are higher with respect to the soot-free systems (0.6 mmol/g_{cat}, 0.77 m mol/g_{cat} and 0.26 mmol/g_{cat} , respectively). This indicates that the presence of soot is beneficial to the NO_x storage performance of all the Ru-K-based catalysts, i.e. regardless of the type of support (e.g. Al, Zr and CZ). Moreover in the presence of soot the NO_x storage capacity of K-containing catalysts is higher than that of the corresponding Ba catalytic formulations.

Of note, the results obtained in the combustion of soot show very different features if compared to Ru-Ba-based catalysts. Indeed, a very huge production of CO_2 is observed in the presence of only oxygen, before the NO addition. Then CO_2 evolution continues during the NO pulse. During the lean phase 67%, 55% and 75% of soot has been oxidized in the case of the Ru-K/Al, Ru-K/Zr and Ru-K/CZ, respectively (vs. 22% and 9% for Ru-Ba/Al and Ru-Ba/CZ). In line with TPO results and with literature [34], this confirms that the substitution of Ba with K promotes the soot combustion activity. This has been ascribed the possible formation of low melting point compounds which improve the mobility of the active surface species and consequently improve the soot combustion activity according to a higher contact between catalysts and soot. Moreover, a synergistic effect between Ru and K which could substantially enhance the efficiency of soot combustion cannot be excluded.

Finally, as expected since most of soot has been removed, the reduction of the stored NO_x is similar to that previously described for the regeneration phase in the absence of soot. Only a small increase in the N_2 selectivity (74%, 83% and 67% for Ru-K/Al, Ru-K/Zr and Ru-K/CZ, respectively in the presence of soot vs. 32%, 71% and 41% in the absence of soot) has been found.

4. CONCLUSIONS

In this work we have investigated the catalytic behavior of Ru-based materials in both soot oxidation and simultaneous removal of soot and NOx, and the results have been compared with that of the model Pt-Ba/Al_2O_3 and Pt-K/Al_2O_3 catalysts.

All the formulations promote the combustion of particulate in the presence of NO/O_2 with remarkable results achieved for potassium-doped materials. The promotion for K-based catalysts

seems to be rather independent on the nature of the support, and it appears to be correlated to a synergic interaction between Ru and K that boosts the combustion of soot at low temperature. Notably, K-containing catalysts exhibit very low onset temperature, in the range 220-235 °C.

All the Ru-based samples are able to simultaneously remove soot and NO_x, when operating under isothermal cycling conditions, i.e. alternating lean-rich phases according to the typical DPNR strategy. In particular, the investigated materials show a storage capacity comparable to that of model Pt-based catalyst. It is worth noticing the increase of NO_x storage capacity over Ru-based systems in presence of particulate, while for model Pt-containing catalysts a detrimental effect of soot is usually found. Among all the developed formulations, K-based materials exhibit higher NO_x storage capacity and higher soot oxidation activity if compared to Ba-containing samples.

In conclusion, the results point out that Ru-based catalysts show interesting properties for the simultaneous removal of soot and NO_x. The performances on NO_x removal and soot combustion revealed by some formulations are remarkable; however, their reactivity in the reduction of the stored NO_x should be further improved, specifically to increase the N_2 selectivity, and investigations are presently ongoing in our labs.

ACKNOWLEDGMENTS: The authors thank financial support from MIUR (Futuro in ricerca, FIRB 2012, project SOLYST). J.L. is Serra Húnter Fellow and is grateful to ICREA Academia program.

References

[1] W.A. Majewski and M.K. Khair, Diesel Emissions and their control, SAE International, Warrendale PA (USA), 2006.

[2] M.V. Twigg, Appl Catal B-Environ, 70 (2007) 2.
[3] D. Fino, Sci Technol Adv Mat, 8 (2007) 93.
[4] B.A.A.L. van Setten, M. Makkee and J.A. Moulijn, Catal Rev, 43 (2001) 489.
[5] M. Shelef and R.W. McCabe, Catal Today, 62 (2000) 35.
[6] A.M. Hernandez-Gimenez, D.L. Castello and A. Bueno-Lopez, Chemical Papers, 68 (2014) 1154.
[7] E. Aneggi, C.d. Leitenburg and A. Trovarelli, Catalysis by Ceria and Related Materials, 2nd Edition, eds. Alessandro Trovarelli and Paolo Fornasiero, Imperial College Press, London, 2013, p. 565.
[8] E. Aneggi, N.J. Divins, C. de Leitenburg, J. Llorca and A. Trovarelli, Journal of Catalysis, 312 (2014) 191.
[9] E. Aneggi, C. de Leitenburg and A. Trovarelli, Catal Today, 181 (2012) 108.
[10] A. Bueno-Lopez, Applied Catalysis B-Environmental, 146 (2014) 1.
[11] C.F. Oliveira, F.A.C. Garcia, D.R. Araujo, J.L. Macedo, S.C.L. Dias and J.A. Dias, Applied Catalysis a-General, 413 (2012) 292.
[12] P.A. Kumar, M.D. Tanwar, S. Bensaid, N. Russo and D. Fino, Chemical Engineering Journal, 207 (2012) 258.
[13] N. Guillen-Hurtado, A. Bueno-Lopez and A. Garcia-Garcia, Applied Catalysis a-General, 437 (2012) 166.
[14] N. Guillen-Hurtado, A. Garcia-Garcia and A. Bueno-Lopez, Appl Catal B-Environ, 174 (2015) 60.
[15] E. Aneggi, D. Wiater, C. de Leitenburg, J. Llorca and A. Trovarelli, Acs Catal, 4 (2014) 172.
[16] M.A. Peralta, M.S. Zanuttini and C.A. Querini, Appl Catal B-Environ, 110 (2011) 90.
[17] K. Shimizu, H. Kawachi, S. Komai, K. Yoshida, Y. Sasaki and A. Satsuma, Catalysis Today, 175 (2011) 93.
[18] E. Aneggi, J. Llorca, C. de Leitenburg, G. Dolcetti and A. Trovarelli, Applied Catalysis B-Environmental, 91 (2009) 489.
[19] K. Tikhomirov, O. Krocher, M. Elsener and A. Wokaun, Applied Catalysis B-Environmental, 64 (2006) 72.
[20] P. Venkataswamy, D. Jampaiah, K.N. Rao and B.M. Reddy, Appl Catal A-Gen, 488 (2014) 1.
[21] B.M. Reddy and K.N. Rao, Catal Commun, 10 (2009) 1350.
[22] Y.H. Zhang, X.T. Zou and L. Sui, Catal Commun, 7 (2006) 855.
[23] H.M. An, C. Kilroy and P.J. McGinn, Catal Today, 98 (2004) 423.
[24] N. Russo, S. Furfori, D. Fino, G. Saracco and V. Specchia, Appl Catal B-Environ, 83 (2008) 85.
[25] M. Weibel, N. Waldbusser, R. Wunsch, D. Chatterjee, B. Bandl-Konrad and B. Krutzsch, Top Catal, 52 (2009) 1702.
[26] E.P.A.N. Toyota Patent, Application No 01107629.6 (2001), European Patent, 2001.
[27] S.H. Koichiro Nakatani, Shinichi Takeshima, Kazuhiro Itoh, Toshiaki Tanaka, Kazuhiko Dohmae, SAE Paper, SP-1674 2002-01-0957 (2002) 8.
[28] J. Klein, I. Fechete, V. Bresset, F. Garin and V. Tschamber, Catal Today, 189 (2012) 60.
[29] K. Krishna and M. Makkee, Catal Today, 114 (2006) 48.
[30] J.A. Sullivan and P. Dulgheru, Appl Catal B-Environ, 99 (2010) 235.

[31] J. Klein, D.L. Wu, V. Tschamber, I. Fechete and F. Garin, Appl Catal B-Environ, 132 (2013) 527.
[32] R. Matarrese, L. Castoldi, N. Artioli, E. Finocchio, G. Busca and L. Lietti, Appl Catal B-Environ, 144 (2014) 783.
[33] L. Castoldi, R. Matarrese, L. Lietti and P. Forzatti, Appl Catal B-Environ, 64 (2006) 25.
[34] R. Matarrese, L. Castoldi, L. Lietti and P. Forzatti, Top Catal, 42-43 (2007) 293.
[35] R. Matarrese, L. Castoldi, L. Lietti and P. Forzatti, Top Catal, 52 (2009) 2041.
[36] L. Castoldi, E. Aneggi, R. Matarrese, R. Bonzi, J. Llorca, A. Trovarelli and L. Lietti, Catal Today, (2015) in press.
[37] V. Choque, N. Homs, R. Cicha-Szot and P.R. de la Piscina, Catal Today, 142 (2009) 308.
[38] Y. Liu, F.Y. Huang, J.M. Li, W.Z. Weng, C.R. Luo, M.L. Wang, W.S. Xia, C.J. Huang and H.L. Wan, J Catal, 256 (2008) 192.
[39] S.X. Yang, Y.J. Feng, J.F. Wan, W.P. Zhu and Z.P. Jiang, Appl Surf Sci, 246 (2005) 222.
[40] J.Y. Qin and K. Aika, Appl Catal B-Environ, 16 (1998) 261.
[41] J. Okal and M. Zawadzki, Appl Catal B-Environ, 89 (2009) 22.
[42] Q.G. Dai, S.X. Bai, X.Y. Wang and G.Z. Lu, Appl Catal B-Environ, 129 (2013) 580.
[43] Y.N. Tchenar, A. Choukchou-Braham and R. Bachir, B Mater Sci, 35 (2012) 673.
[44] R. Blume, M. Havecker, S. Zafeiratos, D. Teschner, E. Vass, P. Schnorch, A. Knop-Gericke, R. Schlogl, S. Lizzit, P. Dudin, A. Barinov and M. Kiskinova, Phys Chem Chem Phys, 9 (2007) 3648.
[45] M. Kurnatowska, W. Mista, P. Mazur and L. Kepinski, Appl Catal B-Environ, 148 (2014) 123.
[46] H.Y. Wang and W.F. Schneider, Phys Chem Chem Phys, 12 (2010) 6367.
[47] L.F. Nascimento, R.F. Martins, R.F. Silva, P.C. de Sousa and O.A. Serra, React Kinet Mech Cat, 111 (2014) 149.
[48] D. Homsi, S. Aouad, J. El Nakat, B. El Khoury, P. Obeid, E. Abi-Aad and A. Aboukais, Catal Commun, 12 (2011) 776.
[49] M. Jeguirim, K. Villani, J.F. Brilhac and J.A. Martens, Appl Catal B-Environ, 96 (2010) 34.
[50] M. Jeguirim, V. Tschamber, K. Villani, J.F. Brilhac and J.A. Martens, Chem Eng Technol, 32 (2009) 830.
[51] S. Aouad, E. Abi-Aad and A. Aboukais, Appl Catal B-Environ, 88 (2009) 249.
[52] M. Dhakad, D. Fino, S.S. Rayalu, R. Kumar, A. Watanabe, H. Haneda, S. Devotta, T. Mitsuhashi and N. Labhsetwar, Top Catal, 42-43 (2007) 273.
[53] A. Pappacena, K. Schermanz, A. Sagar, E. Aneggi and A. Trovarelli, Scientific Bases for the Preparation of Heterogeneous Catalysts: Proceedings of the 10th International Symposium, 175 (2010) 835.
[54] C. Morterra, G. Magnacca, V. Bolis, G. Cerrato, M. Baricco, A. Giachello and M. Fucale, Catalysis and Automotive Pollution Control Iii, 96 (1995) 361.
[55] A. Piras, A. Trovarelli and G. Dolcetti, Appl Catal B-Environ, 28 (2000) L77.
[56] X.D. Wu, S.A. Liu, F. Lin and D.A. Weng, Journal of Hazardous Materials, 181 (2010) 722.
[57] V.G. Milt, E.D. Banus, E.E. Miro, M. Yates, J.C. Martin, S.B. Rasmussen and P. Avila, Chemical Engineering Journal, 157 (2010) 530.
[58] D. Meloni, R. Monaci, M.G. Cutrufello, E. Rombi and I. Ferino, J Therm Anal Calorim, 119 (2015) 1023.

[59] W.L. Xie and J. Chen, J Agr Food Chem, 62 (2014) 10414.
[60] M.B. Cerfontain, R. Meijer, F. Kapteijn and J.A. Moulijn, J Catal, 107 (1987) 173.
[61] S.G. Chen and R.T. Yang, J Catal, 141 (1993) 102.
[62] E. Aneggi, C. de Leitenburg, G. Dolcetti and A. Trovarelli, Catal Today, 136 (2008) 3.
[63] K. Villani, C.E.A. Kirschhock, D. Liang, G. Van Tendeloo and J.A. Martens, Angew Chem Int Edit, 45 (2006) 3106.
[64] L. Di, G.J. Wu, W.L. Dai, N.J. Guan and L.D. Li, Fuel, 143 (2015) 318.
[65] H.Y. Wang and W.F. Schneider, Catal Today, 165 (2011) 49.
[66] L. Castoldi, I. Nova, L. Lietti and P. Forzatti, Catal Today, 96 (2004) 43.
[67] L. Castoldi, L. Lietti, I. Nova, R. Matarrese, P. Forzatti, F. Vindigni, S. Morandi, F. Prinetto and G. Ghiotti, Chemical Engineering Journal, 161 (2010) 416.
[68] L. Castoldi, L. Lietti, P. Forzatti, S. Morandi, G. Ghiotti and F. Vindigni, J Catal, 276 (2010) 335.
[69] L. Castoldi, L. Righini, R. Matarrese, L. Lietti and P. Forzatti, J Catal, 328 (2015) 270.
[70] R. Matarrese, L. Castoldi and L. Lietti, Catal Today, 197 (2012) 228.
[71] L. Lietti, P. Forzatti, I. Nova and E. Tronconi, J Catal, 204 (2001) 175.
[72] N. Artioli, R. Matarrese, L. Castoldi, L. Lietti and P. Forzatti, Catal Today, 169 (2011) 36.
[73] S.J. Jelles, R.R. Krul, M. Makkee and J.A. Moulijn, Catal Today, 53 (1999) 623.
[74] F. Jacquot, V. Logie, J.F. Brilhac and P. Gilot, Carbon, 40 (2002) 335.
[75] A. Setiabudi, M. Makkee and J.A. Moulijn, Applied Catalysis B-Environmental, 50 (2004) 185.
[76] L. Castoldi, N. Artioli, R. Matarrese, L. Lietti and P. Forzatti, Catal Today, 157 (2010) 384.

Figure

Table 1: Composition and BET surface areas of the ruthenium-supported catalysts and the supports

Sample name	Nominal composition	Surface area (m^2/g)
CZ	$Ce_{0.8}Zr_{0.2}O_2$	80
Zr	ZrO_2	60
Al	Al_2O_3	130
Ru-Ba/CZ	Ru(1%)-Ba(10%)/$Ce_{0.8}Zr_{0.2}O_2$	55
Ru-Ba/Zr	Ru(1%)-Ba(10%)/ZrO_2	37
Ru-Ba/Al	Ru(1%)-Ba(10%)/Al_2O_3	123
Ru-K/CZ	Ru(1%)-K(10%)/$Ce_{0.8}Zr_{0.2}O_2$	27
Ru-K/Zr	Ru(1%)-K(10%)/ZrO_2	18
Ru-K/Al	Ru(1%)-K(10%)/Al_2O_3	103

Captions to the Figures

Figure 1: X-ray diffraction profiles of Ru-Ba/MO (A) and Ru-K/MO (B) catalysts (○, $Ce_{0.8}Zr_{0.2}O_2$; □, ZrO_2; △, Al_2O_3; ◊, $BaCO_3$; ∗, KNO_3).

Figure 2: HRTEM images of Ru-Ba/CZ (A) Ru-Ba/Zr (B), Ru-Ba/Al (C), Ru-K/CZ (D) Ru-K/Zr (E) and Ru-K/Al (F).

Figure 3: TPR profiles of Ru-Ba/MO and Ru-K/MO (MO = $Ce_{0.8}Zr_{0.2}O_2$; ZrO_2; Al_2O_3). Inset: production of CH_4 for Ru-K/CZ.

Figure 4: Peak top temperature (°C) for soot combustion in O_2 and NO/O_2 atmosphere.

Figure 5: Adsorption, reduction and thermal desorption phases over (A) Ru-Ba/Al catalyst; (B) Ru-Ba/Zr catalyst; (C) Ru-Ba/CZ catalyst in the absence of soot. Storage phase: 1000 ppm NO + 3% v/v O_2 in He at 350°C; reduction phase: 4000 ppm H_2 in He at 350°C; thermal desorption in He from 350°C up to 500°C (10°C/min).

Figure 6: Adsorption and reduction phases over (A) Ru-K/Al catalyst; (B) Ru-K/Zr catalyst; (C) Ru-K/CZ catalyst in the absence of soot. Storage phase: 1000 ppm NO + 3% v/v O_2 in He at 350°C; reduction phase: 4000 ppm H_2 in He at 350°C.

Figure 7: Adsorption and reduction phases over (A) Ru-Ba/Al catalyst; (B) Ru-Ba/CZ catalyst in the presence of soot. Storage phase: 1000 ppm NO + 3% v/v O_2 in He at 350°C; reduction phase: 4000 ppm H_2 in He at 350°C.

Figure 8: Adsorption and reduction phases over (A) Ru-K/Al catalyst; (B) Ru-K/Zr catalyst; (C) Ru-K/CZ in the presence of soot. Storage phase: 1000 ppm NO + 3% v/v O_2 in He at 350°C; reduction phase: 4000 ppm H_2 in He at 350°C.

Figure 1: X-ray diffraction profiles of Ru-Ba/MO (A) and Ru-K/MO (B) catalysts (○, $Ce_{0.8}Zr_{0.2}O_2$; □, ZrO_2; △, Al_2O_3; ◊, $BaCO_3$; ∗, KNO_3).

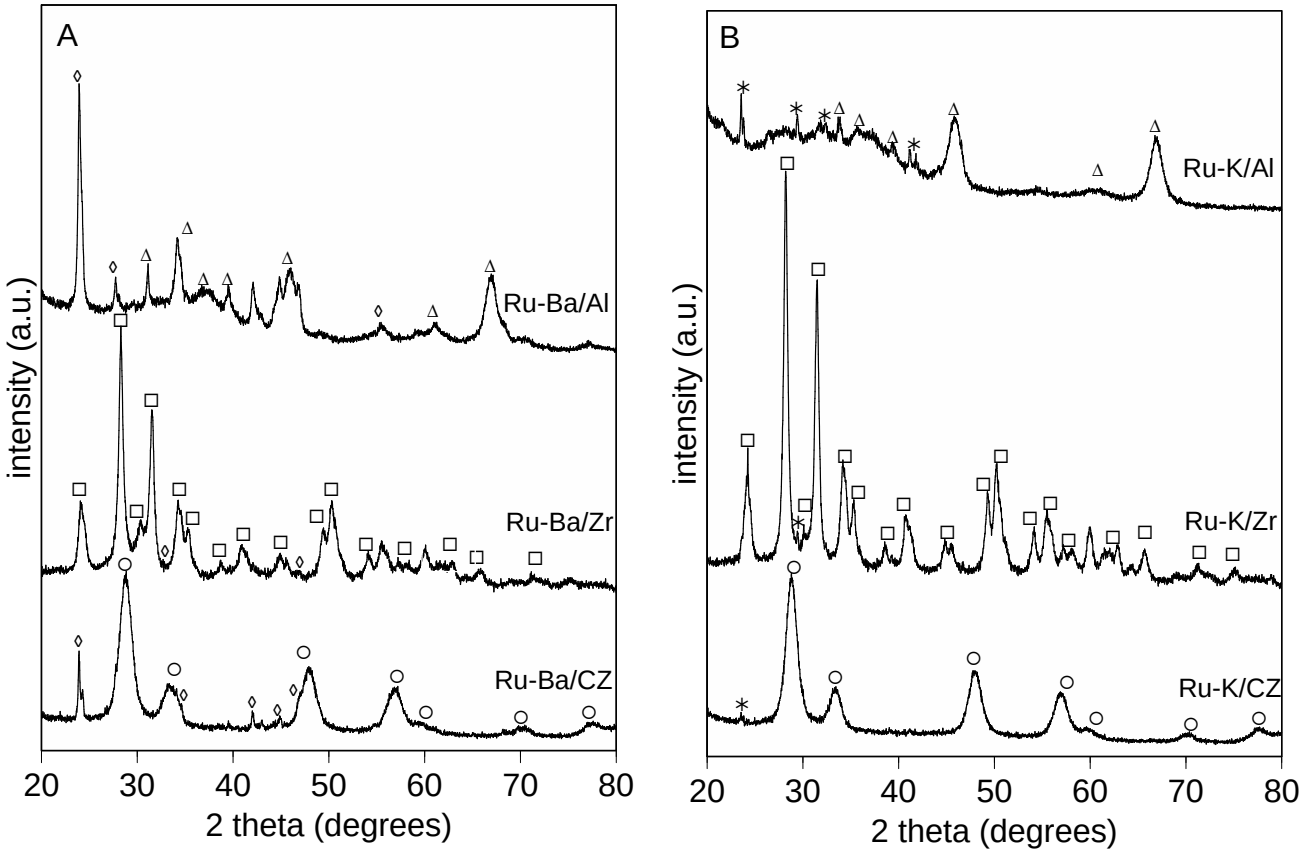

Figure 2: HRTEM images of Ru-Ba/CZ (A) Ru-Ba/Zr (B), Ru-Ba/Al (C), Ru-K/CZ (D) Ru-K/Zr (E) and Ru-K/Al (F).

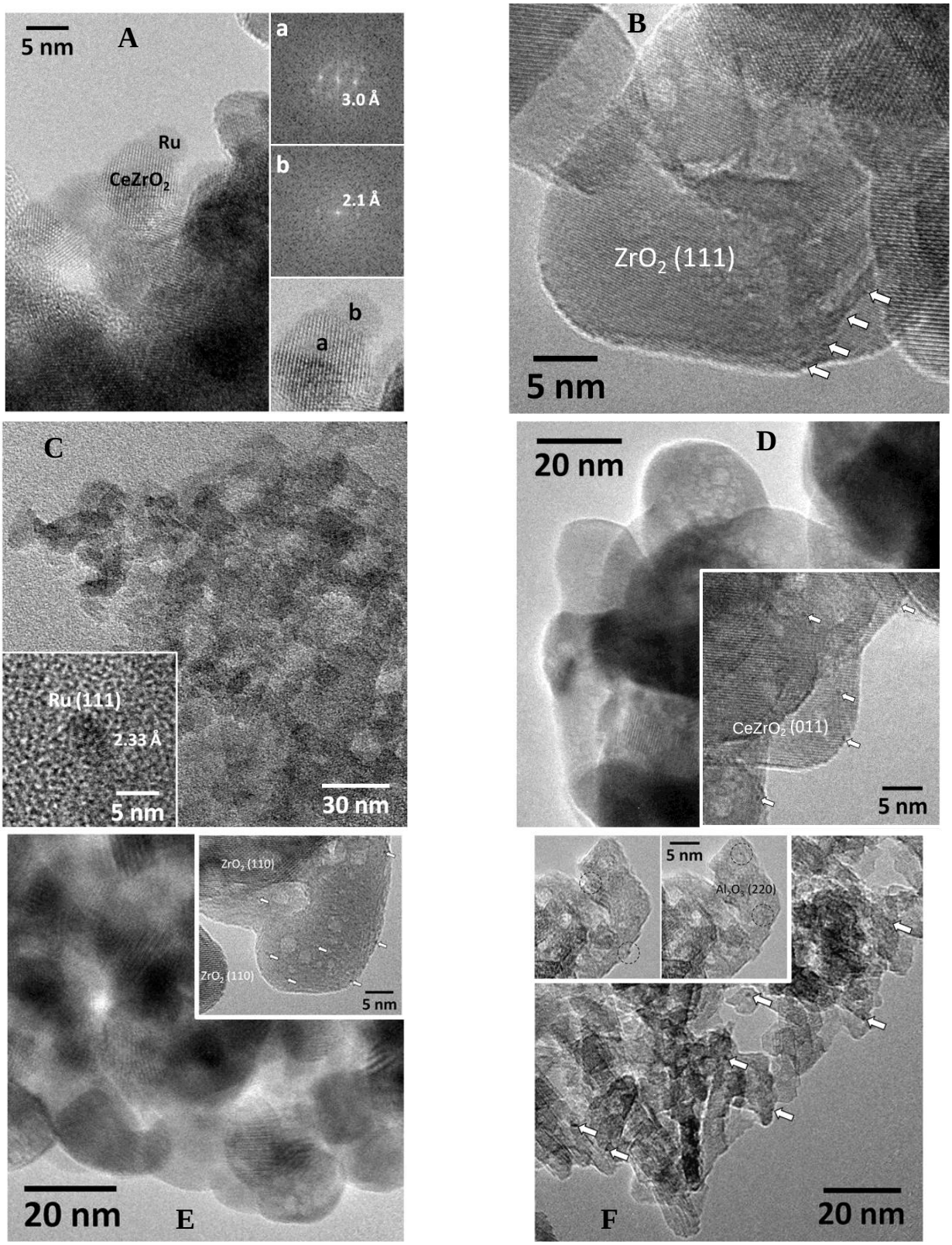

Figure 3: TPR profiles of Ru-Ba/MO and Ru-K/MO (MO = $Ce_{0.8}Zr_{0.2}O_2$; ZrO_2; Al_2O_3). Inset: production of CH_4 for Ru-K/CZ.

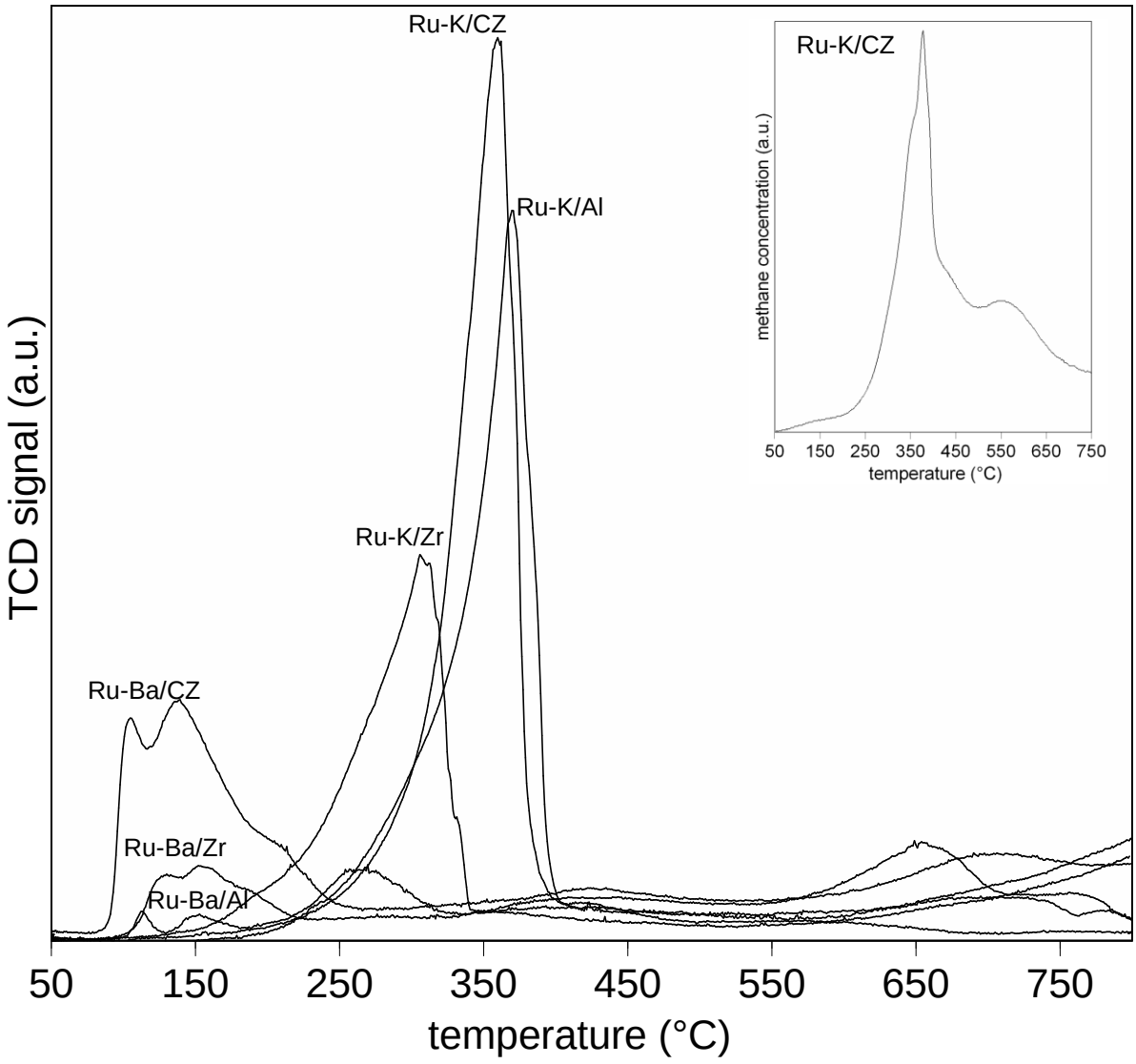

Figure 4: Peak top temperature (°C) for soot combustion in O_2 and NO/O_2 atmosphere.

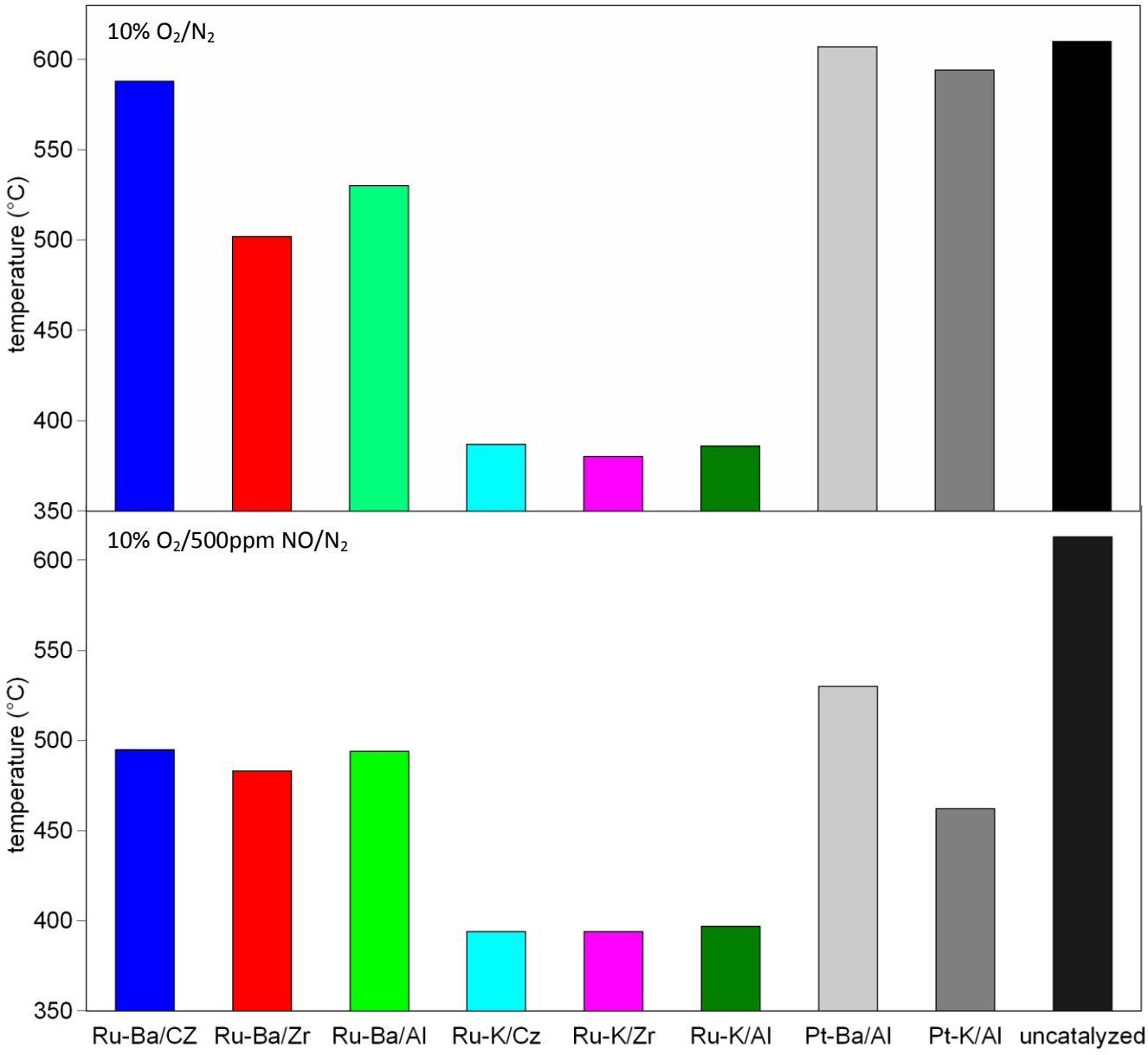

Figure 5: Adsorption, reduction and thermal desorption phases over (A) Ru-Ba/Al catalyst; (B) Ru-Ba/Zr catalyst; (C) Ru-Ba/CZ catalyst in the absence of soot. Storage phase: 1000 ppm NO + 3% v/v O_2 in He at 350°C; reduction phase: 4000 ppm H_2 in He at 350°C; thermal desorption in He from 350°C up to 500°C (10°C/min).

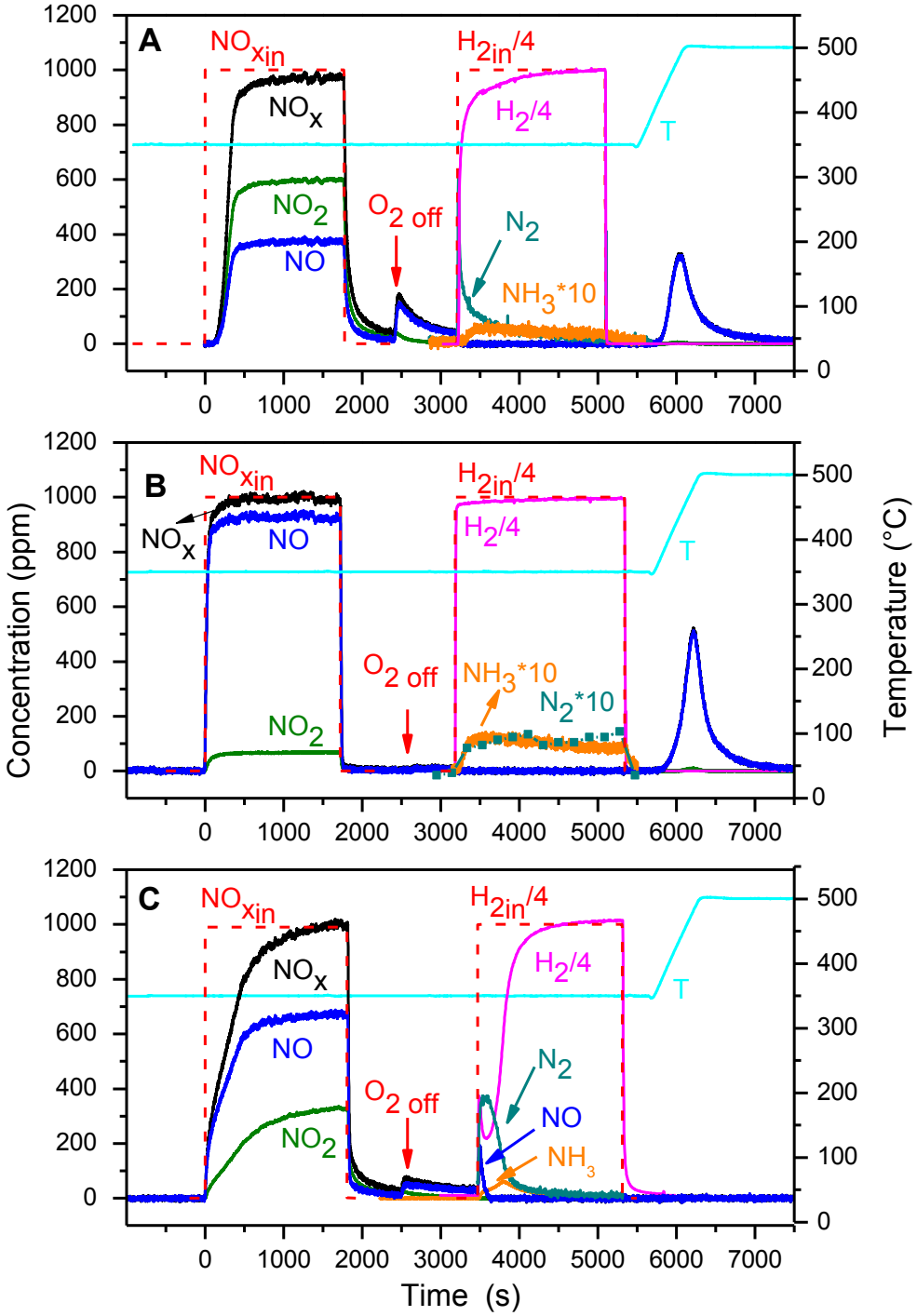

Figure 6: Adsorption and reduction phases over (A) Ru-K/Al catalyst; (B) Ru-K/Zr catalyst; (C) Ru-K/CZ catalyst in the absence of soot. Storage phase: 1000 ppm NO + 3% v/v O_2 in He at 350°C; reduction phase: 4000 ppm H_2 in He at 350°C.

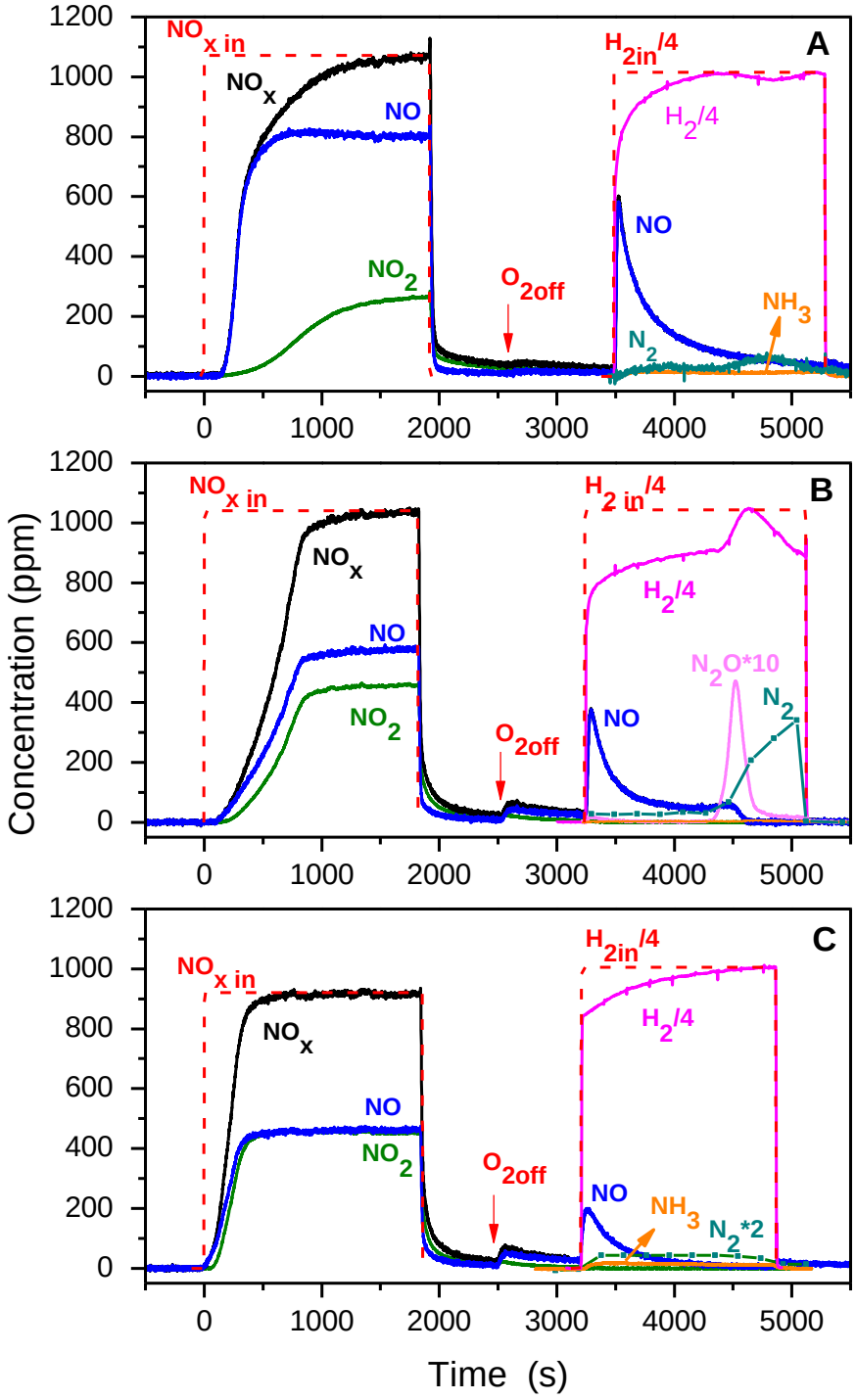

Figure 7: Adsorption and reduction phases over (A) Ru-Ba/Al catalyst; (B) Ru-Ba/CZ catalyst in the presence of soot. Storage phase: 1000 ppm NO + 3% v/v O_2 in He at 350°C; reduction phase: 4000 ppm H_2 in He at 350°C.

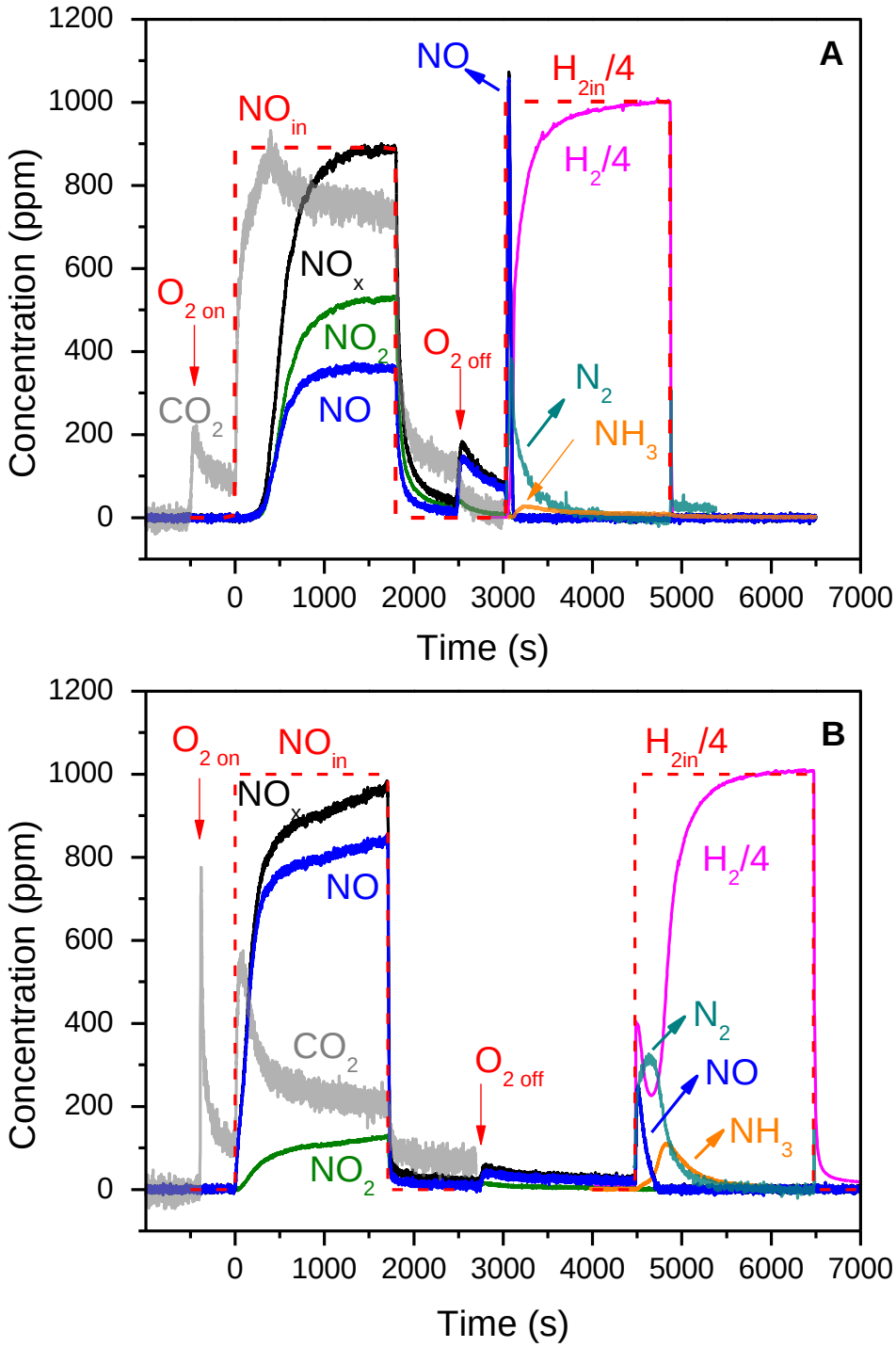

Figure 8: Adsorption and reduction phases over (A) Ru-K/Al catalyst; (B) Ru-K/Zr catalyst; (C) Ru-K/CZ in the presence of soot. Storage phase: 1000 ppm NO + 3% v/v O_2 in He at 350°C; reduction phase: 4000 ppm H_2 in He at 350°C.